Available online at www.sciencedirect.com
SCIENCE DIRECT®
Journal of Solid State Chemistry 177 (2004) 4136–4141
JOURNAL OF SOLID STATE CHEMISTRY
www.elsevier.com/locate/jssc

Structure and physical properties of ternary W_5Si_3-type antimonides and bismuthides $Zr_5M_{1-x}Pn_{2+x}$ (M = Cr, Mn; Pn = Sb, Bi)

Andriy V. Tkachuk, Arthur Mar*

Department of Chemistry, University of Alberta, Edmonton, Alberta, Canada T6G 2G2

Received 16 April 2004; received in revised form 5 August 2004; accepted 8 August 2004
Available online 2 October 2004

Abstract

Four new ternary compounds $Zr_5M_{1-x}Pn_{2+x}$ (M = Cr, Mn; Pn = Sb, Bi) were synthesized by arc-melting and annealing at 800 °C. They crystallize in the tetragonal W_5Si_3-type structure. The crystal structure of $Zr_5Cr_{0.49(2)}Sb_{2.51(2)}$ was refined from powder X-ray diffraction data by the Rietveld method (Pearson symbol $tI32$, tetragonal, space group $I4/mcm$, $Z = 4$, $a = 11.1027(6)$ Å, $c = 5.5600(3)$ Å). Four-probe electrical resistivity measurements on sintered polycrystalline samples indicated metallic behavior. Magnetic susceptibility measurements between 2 and 300 K revealed temperature-independent Pauli paramagnetism for $Zr_5Cr_{1-x}Sb_{2+x}$ and $Zr_5Cr_{1-x}Bi_{2+x}$, but a strong temperature dependence for $Zr_5Mn_{1-x}Sb_{2+x}$ and $Zr_5Mn_{1-x}Bi_{2+x}$ which was fit to the Curie–Weiss law for the latter with $\theta = -11.3$ K and $\mu_{eff} = 1.81(1)$ μ_B. Band structure calculations for $Zr_5Cr_{0.5}Sb_{2.5}$ support a structural model in which Cr and Sb atoms alternate within the chain of interstitial sites formed at the centers of square antiprismatic Zr_8 clusters.

Keywords: Zirconium; Chromium; Manganese; Antimony; Bismuth; Crystal structure; Band structure; Physical properties

1. Introduction

The tetragonal W_5Si_3-type structure is a prevalent one adopted by many metal-rich compounds of the early transition metals and the group 13 or 14 elements [1]. Several ternary compounds containing Sb, a group 15 element, with the W_5Si_3-type structure have now been found in the (Ti, Zr, Hf)–M–Sb (M = transition metal) systems. The first examples were the zirconium-rich antimonides $Zr_5M_{0.5}Sb_{2.5}$ (M = Fe, Co, Ni, Ru, Rh) [2]. Recent investigations have rapidly expanded the number of these ternary zirconium antimonides to $Zr_5Fe_{0.44}Sb_{2.56}$ [3], $Zr_5M_{0.45}Sb_{2.55}$ (M = Cu, Mn) [4,5], and $Zr_5M_{1-x}Sb_{2+x}$ (M = Pd, Cd) [6]. Substitution of zirconium with titanium or hafnium has also been successful, resulting in $Ti_5Fe_{1-x}Sb_{2+x}$ [6,7], $Ti_5M_{0.45}Sb_{2.55}$ (M = Co, Ni) [5,6], $Ti_5M_{1-x}Sb_{2+x}$ (M = Ru, Rh, Pd) [6], $Ti_5M_{0.45}Sb_{2.55}$ (M = Cu, Mn) [8,9], $Hf_5M_{1-x}Sb_{2+x}$ (M = Fe, Co, Ni, Cu, Ru, Rh, Pd) [6], and $Hf_5M_{1-x}Sb_{2+x}$ (M = V, Cr, Mn, Fe, Co, Ni, Cu) [10]. Where crystal structures have been refined, the formula almost invariably deviates from the ideal one that would correspond to the Nb_5SiSn_2-type structure [11], an ordered variant of the W_5Si_3-type structure. This disorder involves the statistical occupation of M and Sb atoms in the $4a$ site, at the center of a square antiprismatic cluster.

We were interested in seeing if this structure type could be extended to include bismuth. Only a few compounds in the (Ti, Zr, Hf)–M–Bi systems are known thus far. The compounds Ti_4MBi_2 (M = Cr, Mn, Fe, Co, Ni) crystallize with the V_4SiSb_2-type structure [12]; $M'_6M''Bi_2$ (M' = Zr, Hf; M'' = Fe, Co, Ni) [13] and Zr_6MnBi_2 [14] are isotypic with an ordered Fe_2P-type structure; Ti_5CuBi_3 and $Ti_{4.34}Zn_{1.23}Bi_3$ belong to the Hf_5CuSn_3 structure type [15].

*Corresponding author. Fax: +1-780-492-8231.
E-mail address: arthur.mar@ualberta.ca (A. Mar).

0022-4596/$ - see front matter © 2004 Elsevier Inc. All rights reserved.
doi:10.1016/j.jssc.2004.08.012

The synthesis of new ternary compounds $Zr_5M_{1-x}Pn_{2+x}$ (M = Cr, Mn; Pn = Sb, Bi) are reported here. The Bi members are the first W_5Si_3-type representatives of their kind. Their crystal structure, electrical and magnetic properties, and band structure are presented.

2. Experimental

2.1. Synthesis

Starting materials were powders of zirconium (99.7%, Cerac), chromium (99.95%, Cerac), manganese (99.95%, Cerac), antimony (99.995%, Aldrich) and bismuth (99.999%, Alfa-Aesar). The compounds were obtained by arc-melting of cold-pressed pellets (~0.5 g) prepared from the elemental components with an excess of 2.5 wt% antimony or 5 wt% bismuth added to compensate for vaporization during the arc-melting under high-purity argon. The ternary compounds were already present in the as-cast alloys; however, the samples were annealed at 800 °C for 1 week in sealed evacuated fused-silica tubes to improve crystallinity. After heat treatment, the ingots were quenched in cold water. Homogeneous samples were also obtained by sintering the cold-pressed pellets for 1 week at 800 °C.

The arc-melted ingots of the ternary compounds have metallic luster; the powders are gray and are stable in air. Energy-dispersive X-ray (EDX) analyses on a Hitachi S-2700 scanning electron microscope did not show the presence of any impurity elements. All samples were characterized by powder X-ray diffraction on an Enraf-Nonius FR552 Guinier camera, recorded with Cu$K\alpha_1$ radiation (λ = 1.54056 Å) using silicon as an external standard. Cell parameters for ternary $Zr_5M_{1-x}Pn_{2+x}$ (M = Cr, Mn; Pn = Sb, Bi) compounds are listed in Table 1.

2.2. Structure determination

All aforementioned ternary compounds belong to the W_5Si_3 structure type [1]. The crystal structure of $Zr_5Cr_{1-x}Sb_{2+x}$ was refined from powder X-ray diffraction data. The sample was prepared by sprinkling on a low-background holder (silicon wafer). Intensity data were collected at room temperature on a Bruker D8 Advance powder diffractometer with monochromated Cu$K\alpha_1$ radiation. Full-profile Rietveld refinements were carried out with use of the program FULLPROF [16]. Further details of the data collection and structure refinement are given in Table 2. Initial atomic positions were taken from the structure of $Zr_5Fe_{0.5}Sb_{2.5}$ [2]. The 4*a* site was allowed to be occupied by a mixture of Cr and Sb atoms. Refinement of the occupancies resulted in a 0.49(2)/0.51(2) distribution of Cr/Sb atoms in this site and full occupancy of the other sites, consistent with the formula $Zr_5Cr_{0.49(2)}Sb_{2.51(2)}$. The final cycle of least-squares refinement included scale factor, background, zero point, cell parameters, pseudo-Voigt peak profile parameters, occupancy, atomic coordinates, and isotropic displacement parameters. The fit of the Rietveld refinement results to the powder pattern is shown in Fig. 1. Final values of the positional and displacement

Table 1
Cell parameters for $Zr_5M_{1-x}Pn_{2+x}$ (M = Cr, Mn; Pn = Sb, Bi)

Compound	a (Å)	c (Å)	V (Å^3)	Reference
$Zr_5Cr_{1-x}Sb_{2+x}$	11.118(2)	5.559(2)	687.2	This work
$Zr_5Mn_{1-x}Sb_{2+x}$	11.099(1)	5.5491(7)	683.6	This work
$Zr_5Mn_{0.45}Sb_{2.55}$	11.068(8)	5.534(5)	677.9	[4]
$Zr_5Cr_{1-x}Bi_{2+x}$	11.286(3)	5.640(2)	718.4	This work
$Zr_5Mn_{1-x}Bi_{2+x}$	11.274(4)	5.629(2)	715.5	This work

Table 2
Crystallographic data for $Zr_5Cr_{0.49(2)}Sb_{2.51(2)}$

Formula	$Zr_5Cr_{0.49(2)}Sb_{2.51(2)}$
Formula mass	787.2
Space group	*I*4/*mcm* (No. 140)
a (Å)	11.1027(6)
c (Å)	5.5600(3)
V (Å^3)	685.38(7)
Z	4
ρ_{calcd} (g cm^{-3})	7.28
Radiation	Cu$K\alpha_1$, λ = 1.54053 Å
2θ range	6–130°
Step width and time	0.02°, 20 s
Number of reflections	182
Number of variables	26
Residuals, R_B, R_F, R_P, R_{WP}	0.049, 0.032, 0.065, 0.087
Goodness of fit, χ^2	0.91

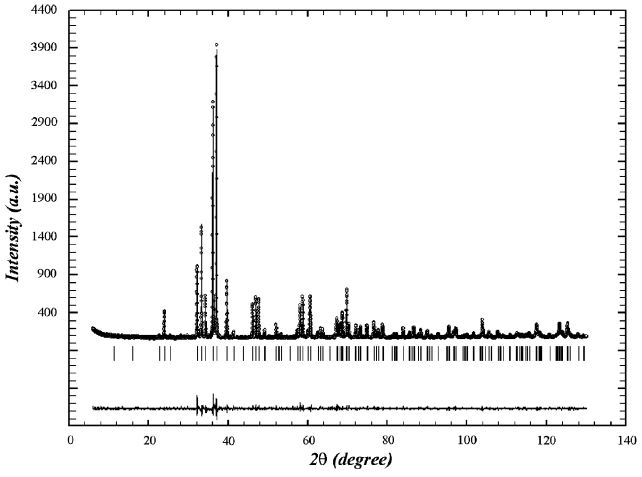

Fig. 1. Rietveld refinement results for $Zr_5Cr_{0.49(2)}Sb_{2.51(2)}$. The observed profile is indicated by circles and the calculated profile by the solid line. Bragg peak positions are located by the vertical tic marks. The difference plot is shown at the bottom.

Table 3
Atomic coordinates and isotropic displacement parameters for $Zr_5Cr_{0.49(2)}Sb_{2.51(2)}$

Atom	Wyckoff position	x	y	z	B_{iso} (Å^2)
Zr1	16*k*	0.0774(2)	0.2159(2)	0	0.53(3)
Zr2	4*b*	0	$\frac{1}{2}$	$\frac{1}{4}$	0.44(6)
X [a]	4*a*	0	0	$\frac{1}{4}$	0.63(6)
Sb	8*h*	0.1633(1)	$x+\frac{1}{2}$	0	0.49(3)

[a] $X = 0.49(2)$ Cr and 0.51 Sb.

Table 4
Interatomic distances (Å) for $Zr_5Cr_{0.49(2)}Sb_{2.51(2)}$

Zr1–*X* [a]	2.901(2) (× 2)	Zr2–Zr2	2.780(1) (× 2)
Zr1–Sb	2.937(2)	Zr2–Sb	2.917(1) (× 4)
Zr1–Sb	2.990(2)	Zr2–Zr1	3.552(2) (× 8)
Zr1–Sb	3.231(1) (× 2)		
Zr1–Zr1	3.245(3)	*X*–*X*[a]	2.780(1) (× 2)
Zr1–Zr1	3.267(1) (× 2)	*X*–Zr1[a]	2.901(2) (× 8)
Zr1–Zr1	3.530(2) (× 2)		
Zr1–Zr2	3.552(2) (× 2)	Sb–Zr2	2.917(1) (× 2)
Zr1–Zr1	3.602(3) (× 2)	Sb–Zr1	2.937(2) (× 2)
		Sb–Zr1	2.990(2) (× 2)
		Sb–Zr1	3.231(1) (× 4)

[a] $X = 0.49(2)$ Cr and 0.51(2) Sb.

parameters are given in Table 3. Interatomic distances are listed in Table 4.

2.3. Electrical resistivity and magnetic susceptibility

Polycrystalline samples of $Zr_5M_{1-x}Pn_{2+x}$ (M = Cr, Mn; Pn = Sb, Bi) were prepared by sintering cold-pressed pellets at 800 °C for 1 week. Their electrical resistivities were measured between 2 and 300 K by standard four-probe techniques on a Quantum Design PPMS system equipped with an *ac* transport controller (Model 7100). The current was 100 μA, and the frequency was 16 Hz. Magnetic susceptibility measurements were made on ground samples (~50 mg) between 2 and 300 K under an applied field of 0.5 T on a Quantum Design 9 T–PPMS dc magnetometer/ac susceptometer. The susceptibility was corrected for contributions for the holder diamagnetism and the underlying sample diamagnetism [17].

2.4. Band structure

Tight-binding extended Hückel band structure calculations were performed with use of the EHMACC suite of programs [18,19]. The atomic parameters are listed in Table 5. Properties were extracted from the band structure using 128 *k*-points in the irreducible portion of the Brillouin zone. Two models were considered: an idealized Zr_5CrSb_2 structure (*I*4/*mcm*) in which the interstitial sites at the centers of Zr_8 square antiprisms are exclusively occupied by Cr atoms, and an idealized $Zr_5Cr_{0.5}Sb_{2.5}$ (or $Zr_{10}CrSb_5$) structure (*I*422) in which they are alternately occupied by Cr and Sb atoms in an ordered fashion.

Table 5
Extended Hückel parameters

Atom	Orbital	H_{ii} (eV)	ζ_{i1}	c_1	ζ_{i2}	c_2
Zr	5*s*	–8.52	1.82			
	5*p*	–4.92	1.78			
	4*d*	–8.63	3.84	0.6207	1.510	0.5793
Cr	4*s*	–8.66	1.70			
	4*p*	–5.24	1.70			
	3*d*	–11.22	4.95	0.5058	1.800	0.6747
Sb	5*s*	–18.8	2.32			
	5*p*	–11.7	2.00			

3. Results and discussion

3.1. Structure

The preparation of the four new ternary zirconium transition-metal pnictides $Zr_5M_{1-x}Pn_{2+x}$ (M = Cr, Mn; Pn = Sb, Bi) having the W_5Si_3-type structure illustrates that this series can be extended to include even heavier pnicogens and earlier transition metals. The substitution with Bi was not obvious, as it may have engendered different matrix effects influencing the ease of inserting the interstitial M atoms within the cluster units of the structure. The range of transition metals that can be inserted in the zirconium antimonide series $Zr_5M_{1-x}Sb_{2+x}$ (M = Cr–Cu) is now almost as wide as in the corresponding hafnium series $Hf_5M_{1-x}Sb_{2+x}$ (M = V–Cu).

The structure of $Zr_5Cr_{0.49}Sb_{2.51}$ is shown in Fig. 2 in a conventional cluster description, normally invoked for W_5Si_3-type structures. It consists of square antiprismatic Zr_8 and tetrahedral Sb_4 clusters with their centers occupied by interstitial atoms. These clusters are condensed by face-sharing and edge-sharing, respectively, to form infinite columns running parallel to the *c*-direction, $^1_\infty[Zr_{8/2}X]$ and $^1_\infty[Sb_{4/2}Zr]$. The interstitial site X within the square antiprismatic cluster is disordered with a nearly 50:50 distribution of Cr and Sb atoms, as is commonly found in related ternary W_5Si_3-type structures. Compared with the sums of the Pauling single-bond radii (Zr–Zr, 2.90; Zr–Cr, 2.64; Zr–Sb, 2.85; Cr–Sb, 2.58; Sb–Sb, 2.80 Å) [20], the interatomic distances are generally reasonable and consistent with those observed in binary antimonides. However, the placement of interstitial atoms within each of the columns imposes a fixed interatomic distance of half the *c* parameter (2.780(1) Å) for the Zr2–Zr2 and *X*–*X*

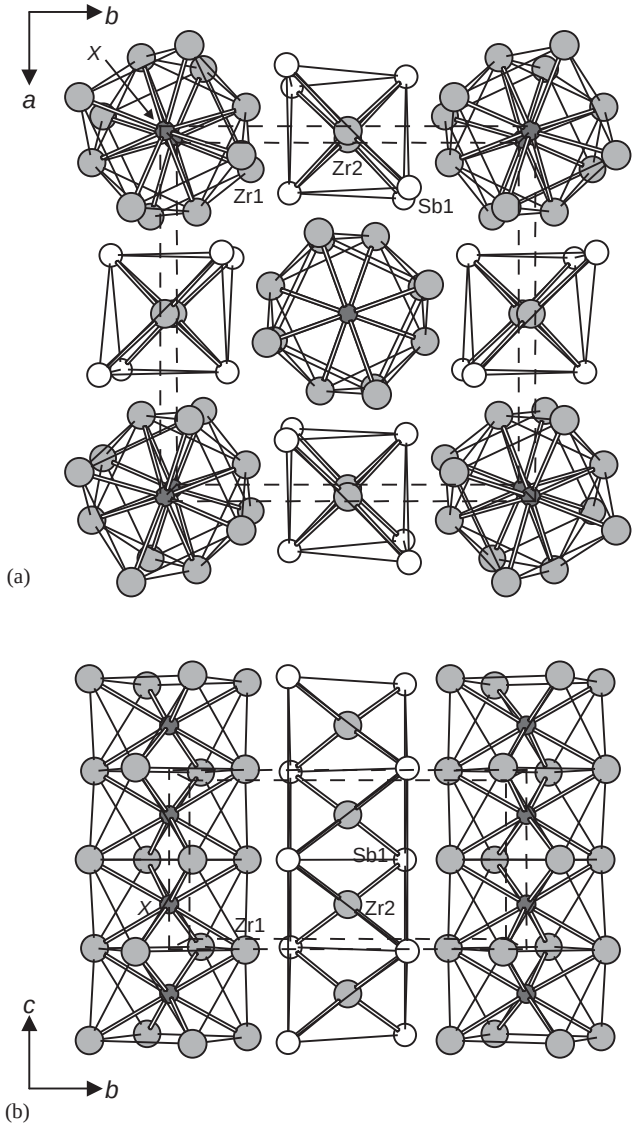

Fig. 2. Structure of $Zr_5Cr_{0.49(2)}Sb_{2.51(2)}$ in terms of square antiprismatic and tetrahedral clusters, viewed (a) down the c axis and (b) as a bounded projection $-\frac{1}{4}<x<\frac{1}{4}$. The large lightly shaded circles are Zr atoms, the small solid circles are X sites (~50% Cr, ~50% Sb), and the medium open circles are Sb atoms.

contacts. For the ternary antimonides, size arguments alone cannot easily distinguish the preference of the X site to be occupied by a transition metal or an Sb atom; moreover, the ~50:50 distribution of Cr:Sb atoms could well be interpreted as a random arrangement of Cr and Sb atoms within each of the $^1_\infty[Zr_{8/2}X]$ columns, or as a local ordering in which Cr and Sb atoms occupy alternate sites within each $^1_\infty[Zr_{8/2}X]$ column, but the columns are out of registry with one another. For the ternary bismuth compounds, the X–X separation ($c/2 \approx 2.82$ Å) would be too short for Bi–Bi contacts, implying a maximum 50% occupancy of Bi atoms in this site and the impossibility of local arrangements of Bi atoms adjacent to each other.

3.2. Properties

Typical plots of the electrical resistivity of pressed pellets of $Zr_5M_{1-x}Pn_{2+x}$ (M = Cr, Mn; Pn = Sb, Bi) are shown in Fig. 3a. They display metallic behavior, but the absolute resistivity values are high and the dependence of resistivity with temperature is slight (the relative resistivity ratios ρ_{300}/ρ_2 are 1.1 for the Cr members and 1.3 for the Mn members). This is consistent with a high residual resistivity arising from the disordered nature of the structure, but grain boundary effects inherent in a pressed pellet will also have a contribution.

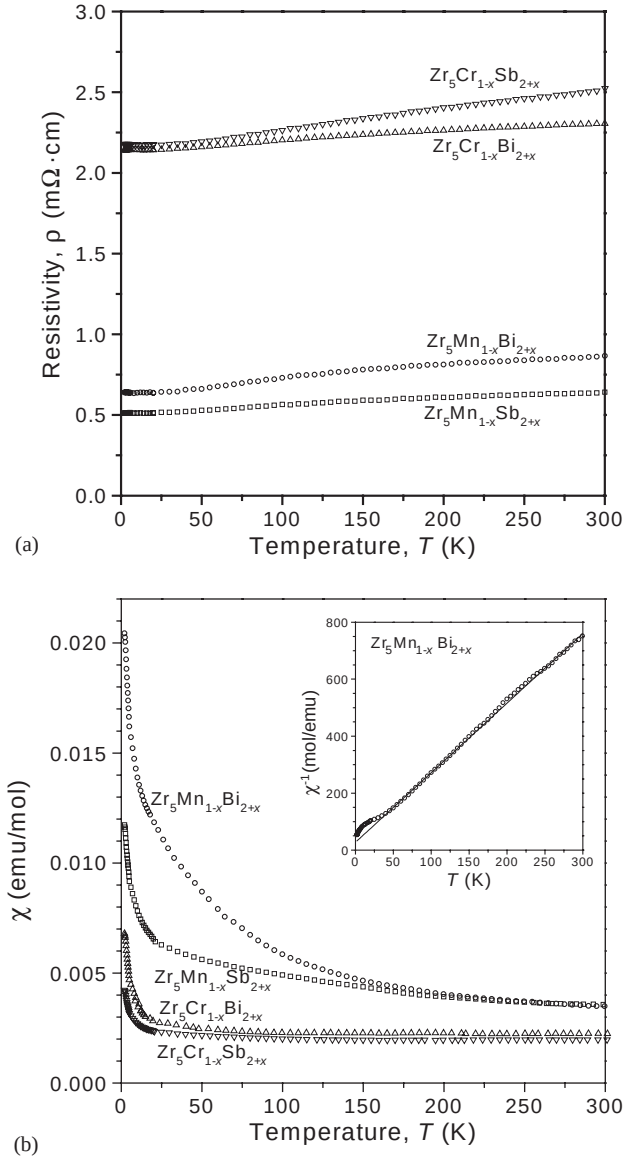

Fig. 3. Plots of (a) electrical resistivity on pressed pellets and (b) dc magnetic susceptibility of powder samples of $Zr_5M_{1-x}Pn_{2+x}$ (M = Cr, Mn; Pn = Sb, Bi). The inset of (b) shows a fit of the data for $Zr_5Mn_{1-x}Bi_{2+x}$ to the Curie–Weiss law, with the temperature-independent susceptibility term subtracted.

Fig. 3b shows that the magnetic susceptibilities of $Zr_5Cr_{1-x}Sb_{2+x}$ and $Zr_5Cr_{1-x}Bi_{2+x}$ are nearly temperature-independent above 25 K, consistent with Pauli paramagnetism. At lower temperatures, the susceptibilities of both compounds increase. Although the Guinier powder patterns revealed single-phase samples, small amounts of paramagnetic impurities are likely responsible for this upturn. In contrast, the magnetic susceptibilities of $Zr_5Mn_{1-x}Sb_{2+x}$ and $Zr_5Mn_{1-x}Bi_{2+x}$ are strongly temperature-dependent. For $Zr_5Mn_{1-x}Sb_{2+x}$, the magnetic susceptibility can be fit by neither the Curie–Weiss nor the modified Curie–Weiss law ($\chi = \chi_o + C/(T-\theta_p)$, where χ_o is associated with the Pauli susceptibility of free charge carriers) in the whole temperature range. At 300 K, the calculated magnetic moment μ_{eff} is 2.93 μ_B. For $Zr_5Mn_{1-x}Bi_{2+x}$, the magnetic susceptibility could be described above 25 K with the modified Curie–Weiss law with $\chi_o = 2.035 \times 10^{-3}$ emu/mol and $\theta_p = -11.3$ K, as seen in the inset of Fig. 3b. The negative Weiss constant suggests antiferromagnetic coupling, but no evidence for long-range order was observed from magnetization data measured above 2 K. From the expression $\mu_{eff} = 2.828[(\chi-\chi_o)(T-\theta_p)]^{1/2}$, the magnetic moment was calculated to be 1.81(1) μ_B. Given the metallic behavior, it is possible that this small moment (equivalent to about one unpaired electron per formula unit) arises from delocalized Mn 3*d* states. Previous measurements and spin-polarized calculations by Kleinke [10] and Tremel [7] on related antimonides suggest that a magnetically ordered ground state is stable for the Fe members and not for the Mn members.

3.3. Bonding

The presence of cluster motifs and the surplus of valence electrons indicate abundant metal–metal bonding in these W_5Si_3-type compounds. This is confirmed by band structure calculations on an idealized $Zr_5Cr_{0.5}Sb_{2.5}$ structure, which reveal the dominance of Zr states at the Fermi level (Fig. 4). There is significant electron transfer from Zr to the more electronegative Cr and Sb atoms, whose states are nearly completely filled up to the Fermi level. The mixing of Zr with Cr and Sb states from –15 eV up to the Fermi level corresponds to strong covalent bonding, as shown by the crystal orbital overlap population (COOP) curves in Fig. 5, with essentially all bonding levels occupied (Mulliken overlap populations (MOP): Zr–Cr, 0.26; Zr–Sb, 0.28). Although most of the Zr–Zr contacts are quite long, up to 3.6 Å, there are many of them, leading to a significant MOP of 0.15. The Zr2–Zr2 contact of 2.780(1) Å is very strong, with a large MOP of 0.40. This distance also dictates the strength of the interactions between atoms occupying the interstitial sites of the square antiprismatic clusters. The model considered here ("$Zr_5Cr_{0.5}Sb_{2.5}$") has a lower total energy, by 13 eV (or ~300 kJ/mol), than one in which Cr atoms occupy exclusively these sites ("Zr_5CrSb_2") because it is more advantageous to optimize polar, heteroatomic Zr–Sb and Cr–Sb bonds than homoatomic Cr–Cr bonds. Similar conclusions were found in the analysis of $Hf_5M_{1-x}Sb_{2+x}$ (M = V, Ni) [10] but interestingly, not in Ti_5FeSb_2 [7]

The metallic behavior and Pauli paramagnetism of $Zr_5Cr_{1-x}Sb_{2+x}$ are confirmed by the location of the Fermi level in a region of large DOS (Fig. 4). Although the experimental values of the magnetic susceptibility can be subject to several sources of error, the calculated values for the density of states at the Fermi level are 41, 78, and 117 e^-/eV for $Zr_5Cr_{0.5}Sb_{2.5}$, $Zr_5Cr_{0.5}Bi_{2.5}$, and $Zr_5Mn_{0.5}Sb_{2.5}$, respectively, consistent with the trend of increasing Pauli paramagnetism in this series (Fig. 4b).

The $Zr_5M_{1-x}Sb_{2+x}$ series has been extended to include the earliest transition metal, Cr, thus far. Given the existence of $Hf_5V_{1-x}Sb_{2+x}$, a worthwhile target is $Zr_5V_{1-x}Sb_{2+x}$. The $Zr_5M_{1-x}Bi_{2+x}$ compounds are the first bismuth representatives, but it remains to be seen if

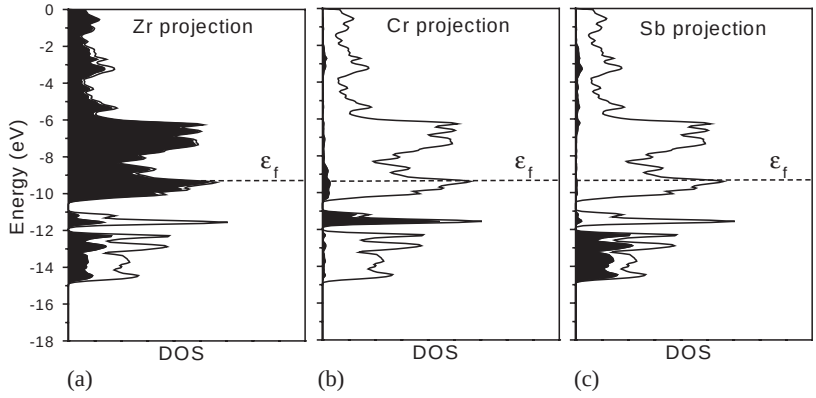

Fig. 4. Contributions of (a) Zr, (b) Cr, and (c) Sb (shaded regions) to the total density of states (DOS) (line) for idealized $Zr_5Cr_{0.5}Sb_{2.5}$. The horizontal line marks the Fermi level ($\varepsilon_f = -9.3$ eV).

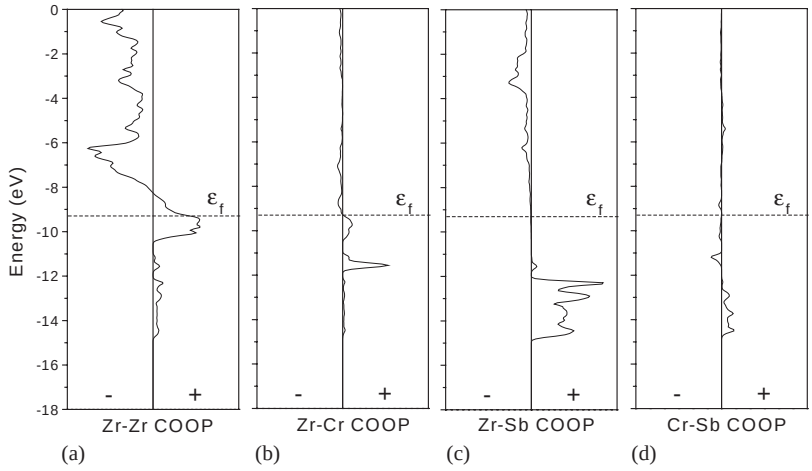

Fig. 5. Crystal orbital overlap population (COOP) curves for (a) Zr–Zr, (b) Zr–Cr, (c) Zr–Sb, and (d) Cr–Sb interactions (< 4.0 Å) in idealized $Zr_5Cr_{0.5}Sb_{2.5}$.

the range of substitution for M is as wide as in other related W_5Si_3-type structures.

Acknowledgments

The Natural Sciences and Engineering Research Council of Canada and the University of Alberta supported this work. We thank Dr. Aniceta Skowron and Dr. James Britten (Brockhouse Institute for Materials Research, McMaster University) for the X-ray data collection and Ms. Christina Barker (Department of Chemical and Materials Engineering) for assistance with the EDX analyses.

References

[1] B. Aronsson, Acta Chem. Scand. 9 (1955) 1107.
[2] Y.-U. Kwon, S.C. Sevov, J.D. Corbett, Chem. Mater. 2 (1990) 550.
[3] G. Melnyk, A. Leithe-Jasper, P. Rogl, R. Skolozdra, J. Phase Equil. 20 (1999) 497.
[4] N. Melnychenko, L. Romaka, Yu. Stadnyk, D. Fruchart, O. Bodak, J. Alloys Compd. 352 (2003) 89.
[5] N.O. Koblyuk, A.V. Tkachuk, L.P. Romaka, Visn. L'viv. Univ. Ser. Khim. 39 (2000) 142.
[6] J.W. Kaiser, W. Jeitschko, Z. Anorg. Allg. Chem. 628 (2002) 337.
[7] G. Melnyk, W. Tremel, J. Alloys Compd. 349 (2003) 164.
[8] N.O. Koblyuk, L.P. Romaka, O.I. Bodak, J. Alloys Compd. 309 (2000) 176.
[9] A. Tkachuk, Yu. Gorelenko, Yu. Stadnyk, B. Padlyak, A. Jankowska-Frydel, O. Bodak, V. Sechovsky, J. Alloys Compd. 319 (2001) 74.
[10] H. Kleinke, C. Ruckert, C. Felser, Eur. J. Inorg. Chem. (2000) 315.
[11] R. Horyń, K. Lukaszewicz, Bull. Acad. Pol. Sci., Ser. Sci. Chim. 18 (1970) 59.
[12] C.G. Richter, W. Jeitschko, B. Künnen, M.H. Gerdes, J. Solid State Chem. 133 (1997) 400.
[13] G. Melnyk, E. Bauer, P. Rogl, R. Skolozdra, E. Seidl, J. Alloys Compd. 296 (2000) 235.
[14] A.G. Bolotaev, A.L. Koroliuk, A.V. Morozkin, V.N. Nikiforov, J. Alloys Compd. 373 (2004) L1.
[15] J.W. Kaiser, M.G. Haase, W. Jeitschko, Z. Anorg. Allg. Chem. 627 (2001) 2369.
[16] J. Rodriguez-Carvajal, FULLPROF: A Program for Rietveld Refinement and Pattern Matching Analysis, version 3.5d, Laboratoire Léon Brillouin (CEA–CNRS), Saclay, France, 1998; based on the original code provided by D. B. Wiles, R. A. Young, J. Appl. Crystallogr. 14 (1981) 149.
[17] L.N. Mulay, E.A. Boudreaux (Eds.), Theory and Applications of Molecular Diamagnetism, Wiley-Interscience, New York, 1976.
[18] M.-H. Whangbo, R. Hoffmann, J. Am. Chem. Soc. 100 (1978) 6093.
[19] R. Hoffmann, Solids and Surfaces: A Chemist's View of Bonding in Extended Structures, VCH Publishers, New York, 1988.
[20] L. Pauling, The Nature of the Chemical Bond, 3rd edition, Cornell University Press, Ithaca, NY, 1960.